Extended flamelet model for LES of non-premixed combustion

By Heinz Pitsch

1. Motivation and objectives

In recent years large-eddy simulation (LES) of turbulent combustion has become a subject of intensive research and modeling efforts. The focus of most activities has been model development using *a priori* studies and LES of simplified flow configurations and chemistry for comparison with direct numerical simulations (DNS). The first application of LES for non-premixed combustion in a turbulent jet flame with detailed comparison with experimental data has recently been conducted by Pitsch & Steiner (1999, 2000). In this study the Lagrangian flamelet model (LFM), first introduced by Pitsch *et al.* (1998), has been used. In this model, rather than using steady state flamelets, unsteady flamelets are solved, which are introduced at the inlet nozzle and assumed to be transported downstream, essentially by convective transport. The time coordinate in the flamelet equations hence becomes a Lagrangian-like time. The scalar dissipation rate appearing as a parameter in the flamelet equations is modeled by its conditional average over cross-sectional planes perpendicular to the jet axis. The model has been applied to the so-called D-flame of the Sandia flame series, experimentally investigated by Barlow & Frank (1998a, 1998b). The results are compared to mean and conditionally averaged temperature and species mass fractions, showing in general very good agreement. However, in the rich part of the flame, mainly CO and H_2 are overpredicted. This has been attributed to the fact that in order to prevent formation of aromatic hydrocarbons, which would interfere with the experimental techniques, the fuel has been diluted with air and is hence partially premixed. This causes the occurrence of heat release in the rich premixed region in the predictions of the LES, which in turn leads to overpredictions of mass fractions of CO, H_2 and other species. Interestingly, similar trends appear in many other modeling studies using the steady flamelet model, the conditional moment closure model, the transported pdf model, and the linear eddy model (Barlow (1998, 1999)), which are mainly used in RANS simulations.

An obvious disadvantage of the LFM as it is applied in Pitsch & Steiner (2000) is that only an averaged scalar dissipation rate is used. This is also the case for most other models, particularly in the context of RANS, where only the time averaged scalar dissipation rate is known. It has been shown in Pitsch & Steiner (2000) that the filtered scalar dissipation rate including the resolved and the sub-grid part in a jet flame is a strongly fluctuating quantity appearing in large-scale organized structures. Figure 1 in Pitsch & Steiner (2000) shows the two-dimensional instantaneous distribution of this quantity from the LES of the Sandia flame D. It is obvious that regions of high scalar dissipation rate might be present on one side of the axis, while the scalar dissipation rate is very low on the other side. This spatial structure is being lost in the cross-sectional conditional averaging procedure applied in Pitsch & Steiner (2000). In recent work we have investigated the influence of fluctuations of the scalar dissipation rate in non-premixed combustion (Pitsch & Fedotov (2000) and Sripakagorn *et al.* (2000)),

showing that these can have a strong impact and can lead to local flame extinction, even if the conditional mean scalar dissipation rate is well below the extinction limit.

In the present work the LFM will be extended to account for local inhomogeneities of the scalar dissipation rate. In the following sections, first the governing equations will be derived and the relation to the flamelet equations derived in earlier work by Peters will be discussed. Following this, the numerical implementation of the resulting equations will be described, and finally, numerical results from the LES of a turbulent jet diffusion flame will be discussed and compared to the results obtained from the LFM and to experimental data.

2. Governing equations

In this section a new formulation of an unsteady flamelet model for LES of non-premixed combustion, the extended flamelet model (EFM), will be developed. The underlying ideas are similar to the LFM, but a different formulation allows for a more detailed consideration of local effects. We will first derive the flamelet equations as proposed by Peters (1983, 1994, 1987). This procedure is very well described, for instance, in Peters (1984), but will still be outlined in this section in order to clearly expose the underlying assumptions. The analysis here will only be discussed for the species mass fractions equations since the derivation for other scalar equations such as the temperature or enthalpy equation can be performed analogously.

We start with the governing equation for mixture fraction Z and species mass fractions Y_i, which can be written as

$$\rho\frac{\partial Z}{\partial t} + \rho\boldsymbol{v}\cdot\nabla Z + \nabla\cdot(\rho D\nabla Z) = 0 \tag{2.1}$$

$$\rho\frac{\partial Y_i}{\partial t} + \rho\boldsymbol{v}\cdot\nabla Y_i + \nabla\cdot(\rho D\nabla Y_i) - \dot{m}_i = 0\,. \tag{2.2}$$

Here, ρ is the density, t the time, $\boldsymbol{v}$ the velocity vector, $\dot{m}_i$ is the chemical source term of species i, and D the molecular diffusivity of the mixture fraction and all chemical species. For simplicity, all Lewis numbers are assumed to be unity for the following derivation of the flamelet equations. Non-constant Lewis numbers can be considered by applying the method of Pitsch & Peters (1998). In order to derive the flamelet equations, we consider the coordinate system introduced in Eqs. (2.1) and (2.2) such that one coordinate, say x_1, at a given instant in time is normal to the surface of stoichiometric mixture. The origin of the coordinate system can be chosen to be traveling with the stoichiometric surface or to be independent of this surface without any implications on the results of the following procedure. According to Peters (1983, 1994, 1987) we then perform a Crocco type coordinate transformation, such that x_1 is replaced by the mixture fraction Z, where the other coordinates remain. The transformation is then given by

$$t, x_1, x_2, x_3 \longrightarrow \tau, Z, Z_2, Z_3\,. \tag{2.3}$$

For this transformation to be valid, x_1 has to be uniquely representable by the new coordinate Z, which is the case in many simplified laminar configurations but is not generally satisfied in a turbulent flow. We therefore have to assume that the reaction zone is smaller than the small scales of the turbulence and restrict the analysis to a small region around the reaction zone. This requirement will be used again in the subsequent derivation and can be called the *flamelet assumption*. Also the possible rotation of the new

coordinate Z with respect to the original coordinate x_1 during the temporal development of the flow field will be neglected. However, it has recently been pointed out by Klimenko (2000) that this error is small if the curvature radius is large compared to the reaction zone thickness, which is the case if the reaction zone is assumed to be thin compared to the turbulent scales.

After this formal transformation, an asymptotic approximation is performed. Again, we invoke the flamelet assumption of a thin reaction zone. Then, changes along mixture fraction iso-surfaces in the vicinity of stoichiometric mixture are small compared to the changes in the direction of the mixture fraction and can be neglected. The resulting equations are the so-called flamelet equations given by

$$\rho\frac{\partial Y_i}{\partial \tau} - \rho\frac{\chi}{2}\frac{\partial^2 Y_i}{\partial Z^2} - \dot{m}_i = 0\,, \tag{2.4}$$

where the scalar dissipation rate χ has been introduced as

$$\chi = 2D\left(\nabla Z\right)^2\,. \tag{2.5}$$

It should be noted that in this equation the newly introduced time τ is the time defined in the new coordinate system, which means that the time derivative $\partial/\partial\tau$ is to be evaluated at constant mixture fraction Z. Hence, τ is a Lagrangian-like time coordinate. With respect to a point in space which is independent of the stoichiometric surface, this new coordinate system moves with the velocity of a point on the stoichiometric surface. The unsteady flamelet model using Eq. (2.4) in a model for turbulent non-premixed combustion has, therefore, been called the Lagrangian Flamelet Model (Pitsch (2000) and Pitsch & Steiner (2000)).

We now want to derive an Eulerian form of the flamelet equations. For the Lagrangian-like time coordinate τ follows

$$\frac{\partial}{\partial \tau} = \frac{\partial}{\partial t} + \frac{\partial x_Z}{\partial t}\cdot\nabla\,, \tag{2.6}$$

where $\partial x_Z/\partial t$ is the velocity of a point on the mixture fraction iso-surface. The velocity of the scalar iso-contours has been discussed in connection with the LFM in Pitsch & Steiner (2000) and can, according to Gibson (1968), be given as

$$\frac{\partial x_Z}{\partial t} = \boldsymbol{v} - \frac{\nabla\cdot(\rho D\nabla Z)}{\left|\nabla Z\right|^2}\nabla Z\,, \tag{2.7}$$

where the first part is because of convection and the second part because of diffusion of the mixture fraction.

Introducing Eqs. (2.6) and (2.7) into Eq. (2.4) and for the reasons discussed in Pitsch & Steiner (2000) neglecting the diffusive part in Eq. (2.7) leads to the flamelet equations in an Eulerian system

$$\rho\frac{\partial Y_i}{\partial t} + \rho\boldsymbol{v}\cdot\nabla Y_i - \rho\frac{\chi}{2}\frac{\partial^2 Y_i}{\partial Z^2} - \dot{m}_i = 0\,. \tag{2.8}$$

The same equations could have been derived using a two-scale asymptotic analysis as recently suggested by Peters (2000). In this approach a short scale is defined in terms of the mixture fraction covering the range in the close vicinity of the flame surface. A second coordinate is assumed to describe variations on the long scales only and essentially replaces the spatial coordinates. Since the long scale coordinate is still Eulerian, the convection term remains during the derivation in the equation, and a transformation as given by Eq. (2.6) is not needed.

Equations 2.8 have been derived to be valid locally and instantaneously. To apply these flamelet equations as a sub-grid combustion model for LES, closure will be achieved as suggested by Pitsch *et al.* (1998). The scalar dissipation rate and the velocity in the flamelet equations will be replaced by the conditional means of the instantaneous local conditionally filtered values of the scalar dissipation rate and the velocity. Consequently, the species mass fractions obtained by solving the flamelet equations are also to be interpreted as conditional mean quantities. This implies that the influence of the sub-grid fluctuations of the scalar dissipation rate and the velocity is small, which excludes the validity of the current model for situations, where local extinction phenomena are important. Note, however, that the sub-grid part of the scalar dissipation rate certainly needs to be accounted for in the model for the filtered scalar dissipation rate.

The flamelet equations derived here show close resemblance to the first order conditional moment closure model (CMC) proposed by Klimenko (1990) and Bilger (1993). Only the turbulent transport term is missing here, which has been omitted because it is small in the present application. However, it could be included in the model by similar arguments as given in section 3.12 in Peters (2000).

The reason for the similarity of the flamelet equations given here and first order CMC is that both models assume the conditional fluctuations to be negligible. In flamelet modeling these fluctuations would be taken into account by averaging over ensembles of flamelets with different scalar dissipation rates and presuming a pdf of the scalar dissipation rate. In contrast to this, in CMC the conditional fluctuations appear as additional unclosed correlations in the CMC equations. These correlations then have to be modeled. Therefore, differences in both models only appear if conditional fluctuations are taken into consideration.

3. Numerical implementation

Unlike the application of steady state flamelet models, which is very straightforward, the numerical implementation of the present model needs some further consideration. The reason for this is that the flamelet equations derived here are time dependent, three-dimensional in space, and also depend on mixture fraction. Also, the intended use of complex chemistry requires solving Eq. (2.8) for a large number of chemical species. It seems, therefore, that the current approach is prohibitive in LES since this is known to be an expensive technique already for simulations of non-reactive flows.

However, an important aspect here is that in a spatially discretized form of Eq. (2.8) we solve in each computational cell not only for scalar values of Y_i, but for the function $Y_i(Z)$. Under the assumptions made earlier, this function is not likely to change rapidly in space. Strong changes of Y_i, however, are to be expected in the direction of Z. Therefore, the spatial discretization of Eq. (2.8) can be much coarser than the resolution of the remaining equations. The present simulations have been performed using a computational mesh in spherical coordinates with $192 \times 110 \times 48$ cells in the downstream (s), radial (θ), and circumferential (ϕ) direction, schematically shown in Fig. 1. The flamelet equations are spatially discretized in the downstream and circumferential direction only, using 48×8 cells. Since the mixture fraction varies mainly in θ-direction, changes of $Y_i(Z)$ with respect to θ are expected to be small. Therefore, for the solution of Eq. (2.8) the θ-direction is assumed to be homogeneous.

In the time discretization of Eq. (2.8), the unsteady term, the diffusion in Z, and the

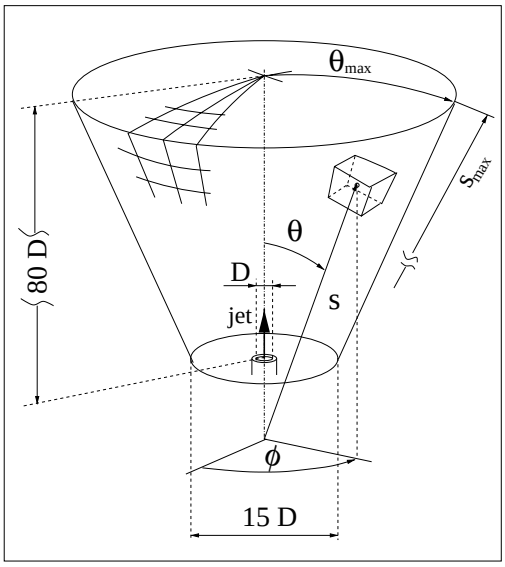

FIGURE 1. Schematic representation of the coordinate system.

chemical source term are solved implicitly. The convection term is explicit and treated as source term in the implicit solution of the remaining terms.

In order to further reduce the computational effort, a reduced 20-step mechanism has been derived for the present simulation. The reduced scheme is based on the GRI 2.11 mechanism by Bowman *et al.* (1998).

4. Results and discussion

In this section numerical results of the presented model will be presented and compared with earlier results obtained by the LFM (Pitsch & Steiner (2000)) and experimental data. Numerical simulations have been performed for a piloted methane/air jet diffusion flame (Sandia Flame D), experimentally investigated by Barlow & Frank (1998a, 1998b). As mentioned earlier, the fuel has been diluted by 75 vol. % of air in order to minimize the formation of polycyclic aromatic hydrocarbons and soot, which would interfere with the applied experimental techniques. The fuel nozzle is enclosed by a broad pilot nozzle and a co-flow of air. The Reynolds number based on the fuel stream is $\mathrm{Re} = 22400$.

The time averaged mixture fraction development along the centerline predicted by the EFM and the LFM is given in Fig. 2 on the left. The overall agreement with the experimental data is very good. The differences between the two models are small and can, particularly in the far downstream part, be attributed to the statistical error, which should disappear for longer sampling time of both simulations. Also shown in Fig. 2 is the time averaged root mean square (RMS) along the centerline. Again the agreement with the experimental data is quite good, and the differences between the models are negligible. These trends were to be expected since the combustion model influences the conserved scalar field only through the density, which already seemed to be predicted quite well in the simulations using LFM and cannot be expected to change largely.

As an example for the main reaction products, centerline profiles of carbon dioxide and water mass fraction are also shown in Fig. 2 as function of the mean mixture fraction. The predictions of the EFM are in very good agreement with the experiments. For CO_2

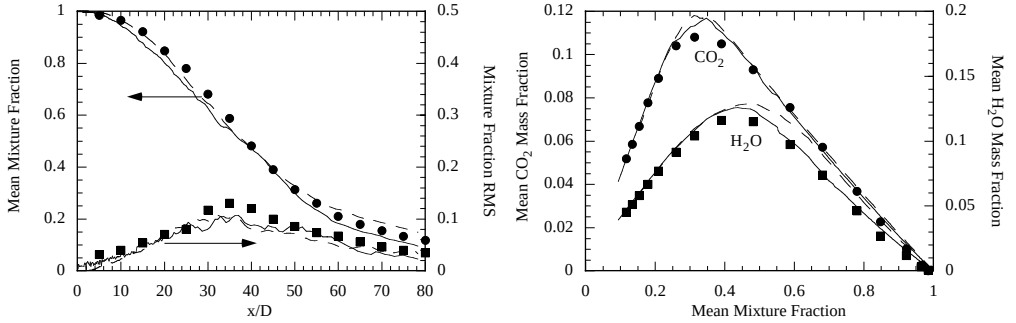

FIGURE 2. Left: Mean and root mean square (RMS) of the mixture fraction along the centerline. Right: Mean temperature and H_2O mass fraction as function of mean mixture fraction along centerline. ——— : EFM; – – – – : LFM; ● ■ : experimental data.

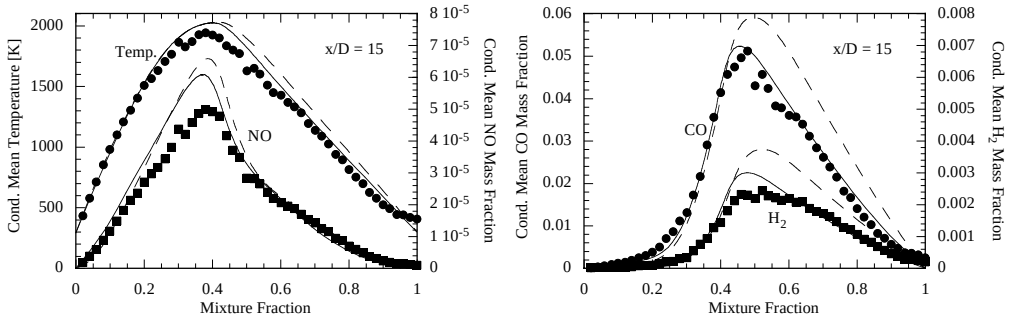

FIGURE 3. Conditional mean averages of temperature, NO, CO, and H_2 mass fractions at $x/D = 15$. ——— : EFM; – – – – : LFM; ● ■ : experimental data.

there are hardly any differences to the LFM. However, for H_2O the new model seems to give some improvement on the fuel rich side, where the mean mixture fraction is larger than 0.45. This corresponds to the region closer to the nozzle. The region with the largest discrepancies between the models is at $\widetilde{Z} \approx 0.6$, which can from the left part of Fig. 2 be estimated to be at $x/D \approx 30$. The reason for these differences will be explained in the following discussion of the conditional averages.

Conditional mean quantities are given in Figs. 3, 4, and 5 at $x/D = 15$, 30, and 45, respectively. Temperature and NO mass fraction are given in the left-hand figures. As stable intermediates CO and H_2 mass fraction are shown in the respective right-hand figures. Again the results of the EFM are compared to the LFM and experimental data.

In the region close to the nozzle, at $x/D = 15$, the maximum temperature can be observed to be slightly overpredicted by both models. This has been discussed by Pitsch & Steiner (2000) in a comparison with the single shot data from the experiments. It has been found that the temperature is well predicted provided the flame is burning. The decreased conditionally averaged temperature found in the experiments is only caused by relatively few local extinction events, which are neglected in both the extended and the Lagrangian flamelet models. On the rich side the temperature is slightly overpredicted by the LFM, but well predicted by the EFM. Also for the NO profile given in Fig. 3 the new model leads to a significant improvement showing very good agreement with the experiments, whereas the predictions by the LFM overpredict the maximum NO concentration slightly. Since NO is well known to be strongly dependent on the temperature, it seems

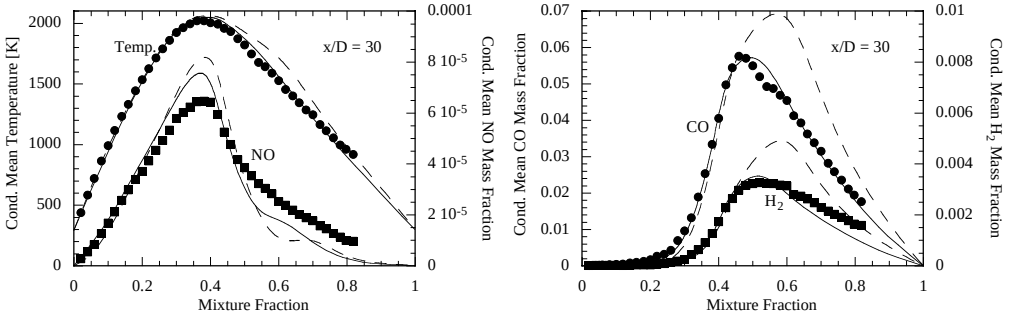

FIGURE 4. Conditional mean averages of temperature, NO, CO, and H_2 mass fractions at $x/D = 30$. ——— : EFM; – – – – : LFM; ● ■ : experimental data.

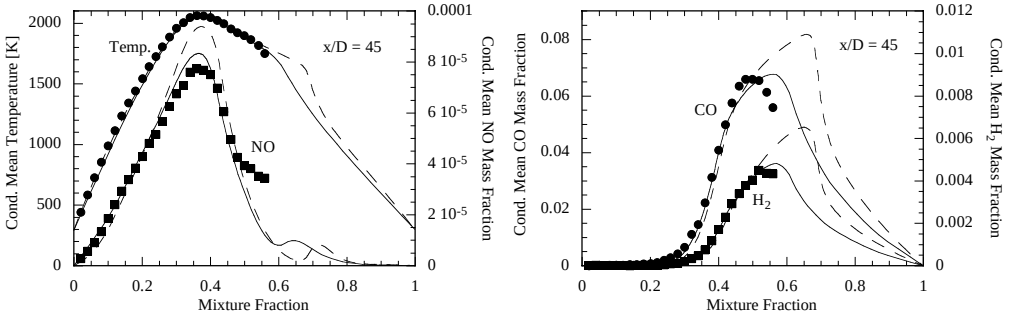

FIGURE 5. Conditional mean averages of temperature, NO, CO, and H_2 mass fractions at $x/D = 45$. ——— : EFM; – – – – : LFM; ● ■ : experimental data.

at first surprising that NO agrees well even though the temperature is overpredicted. The reason is that the high activation temperature of the NO formation causes NO to be formed essentially at the highest temperatures. As explained earlier the local temperature seems to be well predicted and the overprediction of the temperature is only caused by a small volume fraction with significantly lower temperature, which in any case does not contribute to the formation of NO. Similarly to the temperature, but much more obvious, CO and H_2 mass fractions at $x/D = 15$ in the rich part of the flame are also overestimated by LFM. The predictions of the EFM again predict the experimental data very well. The reason for these differences will be explained in the following discussion.

At $x/D = 30$, shown in Fig. 4, the temperature profile predicted by the LFM shows a distinct heat release region approximately $Z = 0.6$. This heat release is caused by the high air content of the fuel stream mentioned earlier. The interaction with the main diffusion flame, located at approximately $Z = 0.35$, causes consumption of fuel and oxidizer, which essentially forms a rich premixed reaction zone. Within this region, because of the high local equivalence ratio, rich stable intermediates such as CO and H_2 are formed in large concentrations as shown in the same figure. However, the rich premixed heat release region cannot be observed in the experimental data. Hence, the temperature in this region is slightly overpredicted, and the CO and H_2 mass fractions are strongly overpredicted.

The main difference between both combustion models discussed here is that in the LFM the scalar dissipation rate is conditionally averaged over cross sections, whereas the EFM is able to take the local fluctuations of the scalar dissipation rate and the unsteady

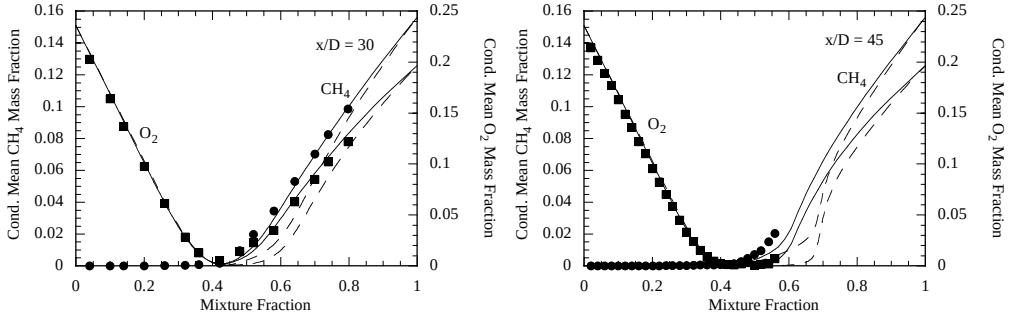

FIGURE 6. Conditional mean averages of temperature, CH_4 and O_2 mass fractions at $x/D = 30$ and $x/D = 45$. ——— : EFM; - - - - : LFM; ● ■ : experimental data.

response of the mixing process and the chemistry into account. The consideration of these fluctuations in the present simulations using the EFM obviously changes the turbulence-chemistry interaction in such a way that chemical reactions in the rich premixed part cannot occur, which is consistent with the experimental findings. Therefore, all quantities predicted by the EFM are in much better agreement with the experimental data. This is reflected in the temperature profile, which does not reveal the rich heat release region as well as in the conditionally averaged mass fractions of the stable intermediates. Both, CO and H_2 mass fraction show excellent agreement with the experiments. For NO this effect does not have a large influence since the mass fraction in the rich part is more governed by transport of NO from the formation region at the maximum temperature, which is only weakly influenced by the rich heat release region, even in the predictions by LFM. However, as shown in Fig. 4, at $Z \approx 0.6$ the LFM predictions reveal an NO consumption region caused by the heat release in this region. Even though NO seems underpredicted even by the results of the EFM, these do not show NO consumption, which is consistent with the experiments. A similar discrepancy as seen in the comparison of NO obtained from the EFM, and the experimental data has been found in a comparison of predictions of a laminar counterflow diffusion flame with experiments using the same fuel (Barlow (2000)), indicating that this underprediction might be caused by the chemical reaction scheme rather than the combustion model.

The observed trends continue for the farther downstream positions. In Fig. 5 the conditionally averaged quantities are given for $x/D = 45$. Here, the heat release in the rich region is even more pronounced in the temperature predictions by the LFM simulation. Interestingly, this can also be observed in a much weaker form in the predictions of the EFM and in the experimental data. This can be very clearly seen in the right-hand figure of Fig. 6, where the conditional averages of methane and molecular oxygen are shown for $x/D = 45$. Obviously the oxygen is depleted not only in the reaction zone of the diffusion flame at $Z = 0.35$, but over a much wider region, ranging from stoichiometric conditions to approximately $Z \approx 0.6$. Also the consumption of fuel starts at higher values of the mixture fraction as compared to $x/D = 30$, which is shown in the left-hand figure of Fig. 6.

The influence of the rich heat release on CO and H_2 at $x/D = 45$ is still quite strong. The results of the EFM again provide significantly improved predictions as compared to the LFM.

5. Conclusions

In the present paper an Eulerian formulation of the unsteady flamelet model for LES of non-premixed combustion is presented, which in contrast to the Lagrangian flamelet model, as formulated in an earlier study, accounts for local fluctuations of the scalar dissipation rate.

The model has been applied to the Sandia flame D and the predictions are compared to results obtained by the LFM and to experimental data. It is demonstrated that inaccuracies in the LFM predictions in the rich part of the flame are mainly because of wrongly predicted heat release in this region. It is shown that the results using the new model formulation provide a significant improvement over the LFM results, and are in excellent agreement with the experimental data.

The main conclusions of this study are that the most important reason for the improvement over the earlier model formulation is the consideration of the locally resolved fluctuations of the modeled scalar dissipation rate and the unsteady response of the interaction of molecular mixing and chemistry.

It seems noteworthy that these fluctuations of the scalar dissipation rate can only be observed in LES-type calculations, which implies that the level of accuracy obtained in the present study cannot be achieved using Reynolds averaged methods.

Acknowledgments

The authors gratefully acknowledge funding by the US Department of Energy in the frame of the ASCI program and by the Center for Turbulence Research.

REFERENCES

Barlow, R. S. (Ed.) 1998 *Proc. of the Third International Workshop on Measurement and Computation of Turbulent Nonpremixed Flames.*

Barlow, R. S. (Ed.) 1999 *Proc. of the Fourth International Workshop on Measurement and Computation of Turbulent Nonpremixed Flames.*

Barlow, R. S. (Ed.) 2000 *Proc. of the Fifth International Workshop on Measurement and Computation of Turbulent Nonpremixed Flames.*

Barlow, R. S. & Frank, J. H. 1998a Effect of Turbulence on Species Mass Fractions in Methane/Air Jet Flames. *Proc. Comb. Inst.* **27**, 1087-1095.

Barlow, R. S. & Frank, J. H. 1998b *www.ca.sandia.gov/tdf/Workshop.html.*

Bilger, R. W. 1993 Conditional moment closure for turbulent reacting flow). *Phys. Fluids A.* **5**, 436.

Bowman, C. T., Hanson, R. K., Davidson, D. F., Gardiner, Jr., W. C., Lissianski, V., Smith, G. P., Golden, D. M., Frenklach, M., Goldenberg, M. 1998 GRI-Mech 2.11. *http://www.me.berkeley.edu/gri_mech/.*

Gibson, C. H. 1968 Fine structure of scalar fields mixed by turbulence. I. Zero-Gradient points and minimal gradient surfaces). *Phys. Fluids.* **11**, 2305.

Klimenko, A. Y. 2000 Private communication.

Klimenko, A. Y. 1990 Multicomponent diffusion of various scalars in turbulent flow. *Prog. Energy Combust. Sci.* **25**, 327-334.

Klimenko, A. Y. & Bilger, R. W. 1999 Conditional moment closure for turbulent combustion. *Prog. Energy Combust. Sci.* **25**, 595-687.

PETERS, N. 1983 Local quenching due to flame stretch and non-premixed turbulent combustion. *Combust. Sci. Tech.* **30**, 1.

PETERS, N. 1984 Laminar diffusion flamelet models in non-premixed turbulent combustion. *Prog. Energy Combust. Sci.* **10**, 319-339.

PETERS, N. 1987 Laminar flamelet concepts in turbulent combustion. *Proc. Combust. Inst.* **21**, 1231-1250.

PETERS, N. 2000 *Turbulent Combustion.* Cambridge University Press.

PITSCH, H., CHEN, M. & PETERS, N. 1998 Unsteady flamelet modeling of turbulent hydrogen/air diffusion flames. *Proc. Combust. Inst.* **27**, 1057-1064.

PITSCH, H. & PETERS, N. 1998 A Consistent Flamelet Formulation for Non-Premixed Combustion Considering Differential Diffusion Effects. *Comb. Flame.* **114**, 26-40.

PITSCH, H. & PETERS, N. 2000 Unsteady Flamelet Modeling of Differential Diffusion in Turbulent Jet Diffusion Flames. *Comb. Flame.* **123**, 358-374.

PITSCH, H. & STEINER, H. 2000 Large-eddy simulation of a turbulent piloted methane/air diffusion flame (Sandia flame D). *Phys. Fluids*, **12**, 2541-2554.

PITSCH, H. & STEINER, H. 2000 Scalar Mixing and Dissipation Rate in Large-Eddy Simulations of Non-Premixed Turbulent Combustion). *Proc. Comb. Inst.*, **28**, to appear.

PITSCH, H. & STEINER, H. 1999 Large-eddy simulation of a turbulent piloted methane/air diffusion flame (Sandia flame D). *Annual Research Briefs*, Center for Turbulence Research, NASA Ames/Stanford Univ. 3-18.

PITSCH, H. & FEDOTOV, S. 2000 Investigation of Scalar Dissipation Rate Fluctuations in Non-Premixed Turbulent Combustion Using a Stochastic Approach). *Comb. Theory Modeling*, submitted.

SRIPAKAGORN, P., KOSÁLY, G. & PITSCH 2000 Local Extinction-Reignition in Turbulent Nonpremixed Combustion. *Annual Research Briefs*, Center for Turbulence Research, NASA Ames/Stanford Univ. This volume, 117-128.